Journal of Solid State Chemistry **159,** 308–320 (2001)
doi:10.1006/jssc.2001.9160, available online at http://www.idealibrary.com on IDEAL®

Synthesis, Structure, and Magnetism of a Series of Self-Assembled Polynuclear Mn(II), Co(II), and Cu(II) Cluster Complexes

Laurence K. Thompson,*,[1] Craig J. Matthews,* Liang Zhao,* Zhiqiang Xu,* David O. Miller,* Claire Wilson,† Michael A. Leech,† Judith A. K. Howard,† Sarah L. Heath,‡ A. Gavin Whittaker,§ and Richard E. P. Winpenny§,[2]

*Department of Chemistry, Memorial University, St. John's, Newfoundland, A1B 3X7, Canada; †Department of Chemistry, University of Durham, Durham DH3 1LE, United Kingdom; ‡Department of Chemistry, University of York, Heslington, York YO10 5DD, United Kingdom; and §Department of Chemistry, University of Edinburgh, West Mains Road, Edinburgh EH9 3JJ, United Kingdom
E-mail: lthomp@morgan.ucs.mun.ca

Received March 20, 2001; accepted March 21, 2001

IN DEDICATION TO THE LATE PROFESSOR OLIVIER KAHN FOR HIS PIONEERING CONTRIBUTIONS TO THE FIELD OF MOLECULAR MAGNETISM

The single-crystal structures and magnetic properties of a series of self-assembled cluster complexes of Mn(II), Co(II), Co(II)/Co(III), and Cu(II), with a group of alkoxy-diazine ligands, which have square and rectangular primary architectures, are reported. In one novel case a secondary coordination sphere of metal ions can be built up on a square core, due to the presence of vacant extra-core coordination sites. $[Mn_4(poapz\text{-}H)_4(H_2O)_4](NO_3)_4 \cdot H_2O$ (1); monoclinic, $C2/c$, $a =$ 21.7120(4) Å, $b = 17.421(4)$ Å, $c = 17.273(4)$ Å, $\beta = 109.34(3)^\circ$. $[Co_4(poap\text{-}H)_2(poap\text{-}2H)_2](NO_3)_4 \cdot 7H_2O$ (3); triclinic, $P\bar{1}$, $a =$ 9.6855(6) Å, $b = 12.9462(7)$ Å, $c = 13.7383(8)$ Å, $\alpha =$ 106.5730(10), $\beta = 99.0400(10)$ Å, $\gamma = 95.737(10)^\circ$. $[Co_4(poapz\text{-}H)_4(H_2O)_4](NO_3)_4 \cdot 2H_2O$ (4); monoclinic, $C2/c$, $a =$ 21.160(2) Å, 17.808(2) Å, $c = 17.000(2)$ Å, $\beta = 106.904(9)^\circ$. $[Co_4(pzoapz\text{-}H)_4(H_2O)_4](ClO_4)_4 \cdot 3H_2O$ (5); monoclinic, $P2_1/a$, $a = 23.24(1)$ Å, $b = 13.681(3)$ Å, $c = 23.37(2)$ Å, $\beta = 118.17(4)^\circ$. $[Cu_4(poap\text{-}H)_4](ClO_4)_4 \cdot CH_3CN \cdot 4.75H_2O$ (6); triclinic, $P\bar{1}$, $a = 13.966(1)$ Å, $b = 14.195(1)$ Å, $c = 19.452(2)$ Å, $\alpha = 83.435(2)^\circ$, $\beta = 80.727(1)^\circ$, $\gamma = 63.023(1)^\circ$. $[Cu_5(3poap\text{-}H)_3(3poap\text{-}3H)](ClO_4)_4 \cdot 7.5H_2O$ (7); triclinic, $P\bar{1}$, $a = 11.8316(12)$ Å, $b =$ 14.7017(16) Å, $c = 21.1527(23)$ Å, $\alpha = 92.401(2)^\circ$, $\beta =$ 104.690(2)°, $\gamma =$ 104.586(2)°. Magnetic properties are interpreted in relation to the structures. The Mn(II) complexes (1, 2) and the Co(II) complexes (4, 5) exhibit intramolecular antiferromagnetic coupling associated with large *M*–O–*M* angles, the $Cu(II)_4$ complex 6 exhibits intramolecular ferromagnetic coupling due to magnetic orbital orthogonality, while the $Cu(II)_5$ complex 7 is best described as a combination of a ferromagnetic trinuclear subunit and an antiferromagnetic dinuclear subunit. © 2001 Academic Press

INTRODUCTION

Advanced materials with potential applications in modern technology, e.g., magnetic recording media, are dependent on the close association of magnetic subunits and the ability of these subunits to communicate magnetically. The synthetic challenge in the area of magnetically concentrated transition-metal complexes is to devise ways of specifically organizing paramagnetic metal ions centers into clusters or grids, and to arrange these polynuclear subunits so that they are capable of extended spin communication. Methods based on simple bridging ligands (e.g., methoxide, hydroxide, alkoxide, oxide, carboxylate) have led to the formation of some interesting high-nuclearity molecular clusters (1–10), some of which have high spin ground states and behave as "single-molecule magnets." However control of the reaction outcome in such an approach is often difficult and mostly the resulting systems are formed serendipitously.

A more rational approach to predetemined molecular architectures uses polyfunctional ligands, with well-designed and judiciously positioned donor pockets, arranged so that self-assembly reactions occur to produce grids and clusters. Significant success has been achieved with polytopic ligands based on pyridazine, pyrimidine, phenoxide, and alkoxide bridging fragments, and 2×2, 3×3, and 4×4 high-nuclearity grids have been produced (11–20). In those cases where paramagnetic transition metal ion centers are involved (14–16) the bridging arrangement within the grids leads to antiferromagnetic coupling in all cases. With copper(II) systems (20), by virtue of the strictly orthogonal bridging connections ferromagnetic coupling prevails.

This report describes the structures and magnetic properties of a series of self-assembled tetranuclear 2×2 grid complexes of manganese(II), cobalt(II), cobalt(III), and

[1] To whom correspondence should be addressed.
[2] Present address: Department of Chemistry, University of Manchester, Oxford Road, Manchester M13 9PL, UK.

0022-4596/01 $35.00

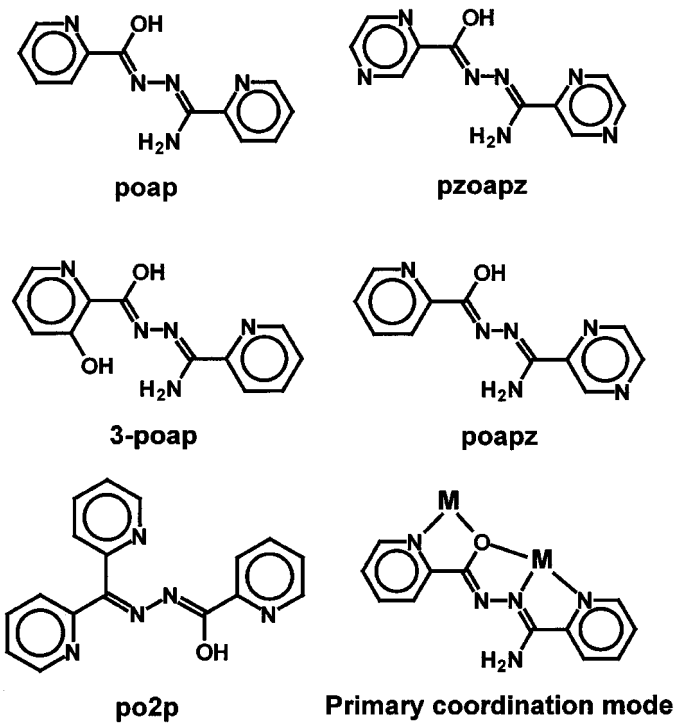

SCHEME 1.

copper(II), and an unusual pentanuclear copper(II) cluster, formed by expansion of a 2×2 core into a second coordination sphere of metal ions. The ligands (Scheme 1) combine terminal pyridine and pyrazine donors on an alkoxy-diazine framework, which provides the primary coordination mode prior to self-assembly.

EXPERIMENTAL

Physical Measurements

Infrared spectra were recorded as Nujol mulls using a Mattson Polaris FT-IR instrument. Microanalyses were carried out by Canadian Microanalytical Service, Delta, Canada. Room temperature magnetic susceptibilities were measured by the Faraday method using a Mettler ME21 microbalance and a Cahn 0.8-T permanent magnet, fitted with Faraday pole caps, and variable temperature magnetic data (2–300 K) were obtained using a Quantum Design MPMS5S SQUID magnetometer with field strengths in the range of 0.1 to 1.0 T. Samples were prepared in aluminum caps, mounted inside the sample straw, and attached to the sample transport assembly. Background corrections for the sample holder and the diamagnetic components of each sample were applied. Calibrations were carried out with a palladium standard cylinder, and possible temperature errors were determined with $[TMENH_2][CuCl_4]$ ($TMENH_2 = (CH_3)_2\ HNCH_2CH_2NH(CH_3)_2^{2+}$) (21).

Synthesis of Ligands

Pzoapz. This sample was prepared in a manner similar to that of poap and poapz (20), by reaction of 2-pyrazine carboxylic acid hydrazide with the methyl ester of iminopyrazine-2-carboxylic acid, to give a yellow crystalline solid (yield 86%; mp. 268–269°C). ^{1}H NMR (300 MHz, DMSO-d_6, 25°C): 10.84 (s, 1H, OH), 9.35 (s, 1H, pyz), 9.22 (s, 1H, pyz), 8.70–8.90 (m, 4H, pyz), 7.21 (s, 2H, NH_2). Mass spectrum (major mass peaks, m/z): 243(M), 226, 225, 196, 164, 138, 108, 106, 79. IR (Nujol mull, cm^{-1}): 3365, 3267, 3198 (ν NH, OH); 1698 (ν C = O); 1657, 1613 (ν C = N). Anal. Calcd for $C_{10}H_9N_7O$: C, 49.38; H, 3.73; N, 40.31. Found: C, 49.21; H, 3.75; N, 40.92.

Po2p. A solution of di-2-pyridyl ketone (1.84 g, 10.0 mmol) in ethanol (10 mL) was added to a solution of picolinic acid hydrazide (1.37 g, 10.0 mmol) in ethanol (40 mL) and the mixture refluxed for 10 h. The volume of the solution was reduced to 20 mL and the resulting white precipitate (2.5 g, 83% yield) was filtered off and recrystallized from absolute ethanol (mp. 162–163°C). Mass spectrum (major mass peaks, m/z): 304(M + 1), 197, 169, 168, 141, 115, 78. IR (Nujol mull, cm^{-1}): 3368, 3195 (ν NH, OH); 1687, 1583, 1564 (ν C = O, C = N), 993 (py). Anal. Calcd for $C_{17}H_{13}N_5O$: C, 67.32; H, 4.32; N, 23.09. Found: C, 67.38; H, 4.34; N, 23.19.

3poap. This sample was prepared in a manner similar to that of pzoapz (20) from the hydrazide of 3-hydroxypicolinic acid and the methyl ester of imino picolinic acid derived from 2-cyanopyridine in MeOH/NaOMe and obtained as a cream-coloured solid (yield 60%, mp. 250–290°C dec.). Anal. Calcd for $C_{12}H_{11}N_5O_2.3H_2O$: C, 46.30; H, 5.50; N, 22.50. Found: C, 46.28; H, 4.84; N, 22.27.

Synthesis of Complexes

$[Mn_4(poapz\text{-}H)_4(H_2O)_4](NO_3)_4 \cdot H_2O$ (**1**). $Mn(NO_3)_2 \cdot 6H_2O$ (0.29 g, 1.0 mmol) was dissolved in water (30 mL) and poapz (20) (0.24 g, 1.0 mmol) added with stirring. The ligand dissolved to give a yellow solution from which an oily solid deposited after one month. The crude product was recrystallized from ethanol containing excess $Mn(NO_3)_2 \cdot 6H_2O$ ($\sim$ 4 equ.) to give red crystals suitable for structural analysis after one week (yield 40%). Anal. Calcd for $[Mn_4(C_{11}H_9N_6O)_4(H_2O)_4](NO_3)_4 \cdot H_2O$: C, 34.71; H, 3.04; N, 25.75. Found: C, 35.00; H, 2.57; N, 25.55. $[Co_4(poapz\text{-}H)_4(H_2O)_4](NO_3)_4 \cdot 2H_2O$ (**4**) was prepared in a similar manner from an aqueous solution using $Co(NO_3)_2 \cdot 6H_2O$ and obtained as red-brown crystals directly from the mother liquor (yield 60%). Anal. Calcd for $[Co_4(C_{11}H_9N_6O)_4\ (H_2O)_4](NO_3)_4 \cdot 2H_2O$: C, 33.95; H, 3.11; N, 25.19. Found: C, 33.90; H, 3.10; N, 24.96. $[Co_4(pzoapz\text{-}H)_4(H_2O)_4](ClO_4)_4 \cdot 3H_2O$ (**5**) was

prepared similarly from $Co(ClO_4)_2 \cdot 6H_2O$ in hot water containing 50% methanol. Dark, almost black crystals were obtained from the mother liquor (yield 50%). Anal. Calcd for $[Co_4(C_{10}H_8N_7O)_4(H_2O)_4]$ $(ClO_4)_4 \cdot 3H_2O$: C, 27.81; H, 2.69; N, 22.72. Found: C, 27.75; H, 2.58; N, 22.81.

$[Mn_4(po2p\text{-}H)_4(H_2O)_2](ClO_4)_4 \cdot 18H_2O$ (**2**). Po2p (0.15 g, 0.5 mmol) was added to a solution of $Mn(ClO_4)_2.6H_2O$ (1.1 g, 3.0 mmol) in $MeCN/H_2O/MeOH$ mixture (10/5/5 mL) and the mixture heated to give a red-orange-coloured solution. Slow evaporation at room temperature gave red crystals (yield 52%). Anal. Calcd for $[Mn_4(C_{17}H_{12}N_5O)_4]$ $(ClO_4)_4 \cdot 18H_2O$: C, 37.97; H, 3.94; N, 13.02. Found: C, 37.35; H, 2.98; N, 12.93.

$[Co_4(poap\text{-}H)_2(poap\text{-}2H)_2](NO_3)_4 \cdot 7H_2O$ (**3**). Poap (20) (0.24 g, 1.0 mmol) was added to a hot aqueous solution (25 mL) of $Co(OAc)_2 \cdot 4H_2O$ (0.25 g, 1.0 mmol) and the mixture stirred until the ligand dissolved, giving a deep purple solution. A saturated solution of $NaNO_3$ (3.0 g in 10 mL water) was added and the heating continued for several minutes. The solution was cooled to room temperature and filtered. Deep brown crystals suitable for X-ray analysis formed after one week (yield 65%). Anal. Calcd for $[Co_4(C_{12}H_{10}N_5O)_2$ $(C_{12}H_9N_5O)_2$ $(H_2O)_4](NO_3)_4 \cdot 7H_2O$: C, 36.70; H, 3.46; N, 21.40. Found: C, 36.88; H, 3.01; N, 21.43.

$[Cu_4(poap\text{-}H)_4](ClO_4)_4 \cdot CH_3CN \cdot 4.75H_2O$ (**6**). Compound **6** was prepared as described previously (20), and recrystallized from H_2O/CH_3CN (1 : 4) to give green crystals suitable for X-ray analysis.

$[Cu_5(3poap\text{-}H)_3(3poap\text{-}3H)]$ $(ClO_4)_4 \cdot 7.5H_2O$ (**7**). 3poap (0.26 g, 1.0 mmol) was added to a hot solution of $Cu(ClO_4)_2 \cdot 6H_2O$ (1.1 g, 3.0 mmol) in water/methanol (10/20 mL) with stirring. The green solution was cooled to room temperature and filtered. Dark green crystals suitable for X-ray analysis formed after two weeks (yield 45%). Anal. Calcd for $[Cu_5(C_{12}H_{10}N_5O_2)_3(C_{12}H_8N_5O_2)](ClO_4)_4 \cdot 7.5H_2O$: C, 30.77; H, 2.85; N, 14.95. Found: C, 30.87; H, 2.61; N, 14.73.

Single–Crystal Structure Determinations

Crystallography. Crystal data and information about the data collection and structural refinement for **1** and **3–7** are given in Table 1. Diffraction data for single crystals of **1–3** were collected using a Bruker SMART CCD diffractometer, equipped with an Oxford Cryostream N_2 cooling device (22), with graphite monochromated Mo$K\alpha$ radiation. Cell parameters were determined and refined using the SMART software (23a), raw frame data were integrated using the SAINT program (23b), and the structures were

TABLE 1

Crystallographic Parameters for $[Mn_4(poapz\text{-}H)_4(H_2O)_4](NO_3)_4 \cdot H_2O$ (1), $[Co_4(poap\text{-}H)_2(poap\text{-}2H)_2](NO_3)_4 \cdot 7H_2O$ (3), $[Co_4(poapz\text{-}H)_4(H_2O)_4](NO_3)_4 \cdot 2H_2O$ (4), $[Co_4(pzoapz\text{-}H)_4(H_2O)_4](ClO_4)_4 \cdot 3H_2O$ (5), $[Cu_4(poap\text{-}H)_4](ClO_4)_4 \cdot CH_3CN \cdot 4.75H_2O$ (6)

	1	**3**	**4**	**5**	**6**
Empirical formula	$C_{44}H_{36}Mn_4N_{28}O_{16}$	$C_{50}H_{62}Co_4N_{24}O_2$	$C_{44}H_{50}Co_4N_{28}O_{23}$	$C_{40}H_{47}Co_4Cl_4N_{28}O_{27.5}$	$C_{50}H_{52.5}Cl_4Cu_4N_{21}O_{24.75}$
Formula weight	1432.77	1650.96	1574.79a	1737.53	1739.59
a (Å)	21.720(4)	9.6855(6)	21.160(2)	23.24(1)	13.966(1)
b (Å)	17.421(4)	12.9462(7)	17.808(2)	13.681(3)	14.195(1)
c (Å)	17.273(4)	13.7383(8)	17.000(2)	23.37(2)	19.452(2)
α (°)	90	106.5730(10)	90	90	83.435(2)
β (°)	109.34(3)	99.0400(10)	106.904(9)	118.17(4)	80.727(1)
γ (°)	90	95.737(10)	90	90	63.023(1)
V (Å^3)	6167(2)	1611.39(16)	612991)	6550(6)	3387.9(4)
Z	4	1	4	4	2
Space group	$C2/c$	$P\bar{1}$	$C2/c$	$P2_1/a$	$P\bar{1}$
T (°C)	293(2)	150(2)	299(2)	299(2)	193(1)
λ (Mo$K\alpha$) (Å)	0.71073	0.71073	0.71069	0.71069	0.71073
ρ_{calc} (g/cm^3)	1.543	1.701	1.706	1.762	1.705
μ (cm^{-1})	8.87	11.15	11.67	12.63	14.91
Total data	40508	8717	7497	16123	16898
Observed data[a]	7060	5613	4443	8439	13724
Parameters	491	532	415	907	1009
min., max., $\Delta\rho$ (e/Å^3)	− 0.982, 1.553	− 1.119, 1.731	− 0.83, 1.50	− 0.74, 0.75	− 0.61, 1.06
$R(R_1)$	0.0640(R_1/F^2)	0.0648(R_1/F^2)	0.063(R/F)	0.056(R/F^2)	0.052(R_1/F_2)
R_w(wR_2)	0.1950(wR_2)	0.1906(wR_2)	0.064(R_w)	0.054(R_w)	0.154(wR_2)

[a] $I > 2\sigma(I)$. Rigaku data: $R = \sum||F_o| - |F_c||/\sum|F_o|$, $R_w = [(\sum w(|F_o| - |F_c|)^2/\sum wF_o^2)]^{1/2}$. Siemens smart data: $R_1 = \sum||F_o| - |F_c|/\sum|F_o|$. $wR_2 = [\sum[w(|F_o|^2 - |F_c|^2)^2]/\sum[w(|F_o|^2)^2]]^{1/2}$.

solved using Direct Methods and refined by full-matrix least squares on F^2 using SHELXTL (24, 25). Nonhydrogen atoms were refined with anisotropic atomic displacement parameters (adps). Hydrogen atoms were placed in geometrically calculated positions with isotropic adps 1.2 times that of the parent atom. Disorder problems encountered during the refinement of the structure of **2** prevent reporting full structural details at this time.

Diffraction data were obtained for a red irregular crystal of **4** of dimensions $0.40 \times 0.30 \times 0.50$ mm with a Rigaku AFC6S diffractometer with graphite monochromated Mo$K\alpha$ radiation. Cell constants were obtained from a least-squares refinement of the setting angles of 20 carefully centered reflecions in the range $32.95^\circ < 2\theta < 39.27^\circ$. The structure was solved by direct methods (26) and expanded using Fourier techniques (27). Some nonhydrogen atoms were refined anisotropically, while the rest were refined isotropically. Hydrogen atoms were included but not refined. The final cycle of full-matrix least-squares refinement on F was based on 4443 observed reflections ($I > 2.00\sigma(I)$) and 415 variable parameters. The maximum and minimum peaks on the final difference Fourier map corresponded to 1.50 and -0.83 e/Å^3 respectively. Neutral atom scattering factors were taken from Cromer and Waber (28). Anomalous dispersion effects were included in F_{calc} (29). All calculations were performed using the teXsan (30) crystallographic software package of Molecular Structure Corporation. Compound **5** was treated in a similar way.

Diffraction data for a green prismatic crystal of **6**, of dimensions $0.40 \times 0.10 \times 0.10$ mm, were collected with a Bruker P4/CCD diffractometer with graphite monochromated Mo$K\alpha$ radiation and a rotating anode generator. The full hemisphere of data was collected with 30-s, 0.3° frames to a maximum 2θ value of 52.8°. The data were corrected for Lorentz and polarization effects. The structure was solved by direct methods (31) and expanded using Fourier techniques (26). The nonhydrogen atoms were refined anisotropically. The final cycle of full-matrix least-squares refinement on F^2 was based on 13,724 observed reflections and 1009 variable parameters. The maximum and minimum peaks on the final difference Fourier map corresponded to 1.06 and -0.61 e/Å^3, respectively. Neutral atom scattering factors were taken from Cromer and Waber (28). Anomalous dispersion effects were included in F_{calc} (29). All calculations were performed using the teXsan (30) crystallographic software package of the Molecular Structure Corporation except for refinement, which was performed using SHELXL-97 (31).

Compound **7** was treated in a similar manner, but refinement problems prevent the reporting of full structural details at this time ($R_1 = 0.069$; $wR_2 = 0.1950$). Five copper centers (Cu(1)–Cu(5)) have been located successfully at unit occupancy, with small levels of residual electron density appearing at three other copper locations (Cu(6)–Cu(8)), in sensible agreement with chemical predictions (*vide supra*). This has enabled us to define a logical cluster fragment, in agreement with magnetic and other properties. However full occupancy of the four perchlorate sites predicted from elemental chemical analysis is not fully consistent with the current refinement. This has no bearing on the interpretation of the magnetic properties associated with the cluster itself (*vide infra*).

Crystallographic data for the structures reported in this paper (.cif files) have been deposited with the Cambridge Crystallographic Data Center as supplementary publication CCDC 156924-156928. Copies of the data can be obtained free of charge on application to CCDC, 12, Union Road, Cambridge CB2 1EZ, UK (fax: (+44)1223-336-033; e-mail: deposit@ccdc.cam.ac.uk).

RESULTS AND DISCUSSION

Crystal Structure of $[Mn_4(poapz\text{-}H)_4(H_2O)_4](NO_3)_4 \cdot H_2O$ (**1**)

A structural representation of the cation in **1** is shown in Fig. 1, and selected distances and angles are listed in Table 2. Four pseudo-octahedral Mn(II) centers are bound simultaneously to four deprotonated ligands arranged in two roughly eclipsed parallel pairs above and below the pseudo-planar $Mn_4(\mu\text{-}O)_4$ grid. The core of the structure (Fig. 2) involves four manganese centers bridged by alkoxide oxygen atoms with Mn–O–Mn angles in the range 127.9°–129.3°, and Mn–Mn separations in the range 3.91–3.97 Å. Mn–N (2.15–2.40 Å) and Mn–O (2.15–2.21 Å) distances are typical for Mn(II) complexes.

Each ligand is tetradentate, but provides donors for five metal ion coordination sites because the alkoxide oxygens act as bridges. The total coordination capacity of the four

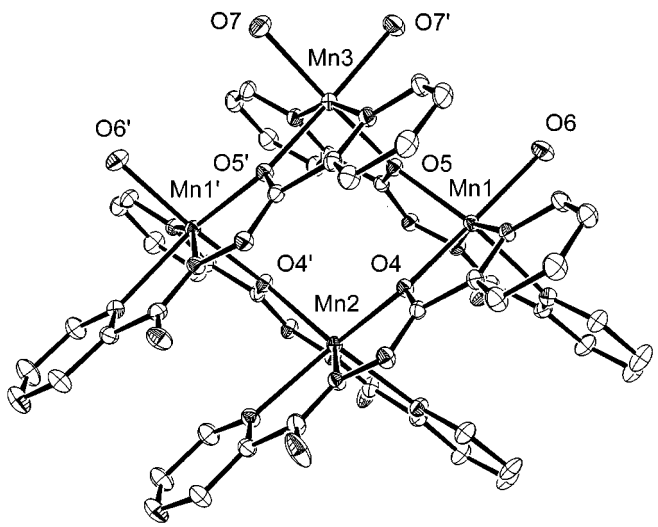

FIG. 1. Structural representation of the cation in **1** (40% probability thermal ellipsoids).

TABLE 2
Bond Lengths (Å) and Angles (°) for $[Mn_4(poapz\text{-}H)_4(H_2O)_4](NO_3)_4 \cdot H_2O$ (1)

Mn(1)–O(4)	2.150(2)	O(4)–Mn(1)–N(11)	75.12(8)
Mn(1)–N(4)	2.154(2)	O(4)–Mn(1)–N(11)	158.23(9)
Mn(1)–O(6)	2.174(2)	O(6)–Mn(1)–N(11)	86.61(9)
Mn(1)–O(5)	2.208(2)	O(5)–Mn(1)–N(11)	128.74(8)
Mn(1)–N(11)	2.231(3)	O(4)–Mn(1)–N(3)	97.44(8)
Mn(1)–N(3)	2.392(2)	N(4)–Mn(1)–N(3)	70.12(9)
Mn(2)–N(9)	2.155(2)	O(6)–Mn(1)–N(3)	88.80(10)
Mn(2)–O(4)	2.202(2)	O(5)–Mn(1)–N(3)	141.78(8)
Mn(2)–N(8)	2.380(2)	N(11)–Mn(1)–N(3)	89.44(9)
Mn(3)–O(5)	2.177(2)	N(9)#1–Mn(2)–N(9)	152.62(13)
Mn(3)–O(7)	2.185(2)	N(9)#1–Mn(2)–O(4)	71.65(8)
Mn(3)–N(12)	2.234(2)	N(9)–Mn(2)–O(4)	126.20(8)
Mn(1)–Mn(2)	3.910(1)	N(9)#1–Mn(2)–O(4)#1	126.20(8)
Mn(1)–Mn(3)	3.962(1)	O(4)–Mn(2)–O(4)#1	08.69(10)
O(4)–Mn(1)–N(4)	99.51(8)	N(9)#1–Mn(2)–N(8)	93.17(9)
O(4)–Mn(1)–O(6)	160.57(8)	N(9)–Mn(2)–N(8)	69.61(9)
N(4)–Mn(1)–O(6)	99.92(9)	O(4)–Mn(2)–N(8)	87.33(8)
O(4)–Mn(1)–O(5)	91.84(7)	O(4)#1–Mn(2)–N(8)	140.19(8)
N(4)–Mn(1)–O(5)	71.80(8)	O(4)#1–Mn(2)–N(8)#1	87.33(8)
O(6)–Mn(1)–O(5)	94.56(8)	N(8)–Mn(2)–N(8)#1	103.52(12)
O(5)–Mn(3)–O(5)#1	96.64(10)		
O(5)–Mn(3)–O(7)#1	89.28(10)		
O(5)–Mn(3)–O(7)	169.80(9)		
O(5)#1–Mn(3)–O(7)	89.28(10)		
O(7)#1–Mn(3)–O(7)	86.1(2)		
O(5)–Mn(3)–N(12)#1	74.86(8)		
O(7)–Mn(3)–N(12)#1	96.53(10)		
O(5)–Mn(3)–N(12)	93.76(8)		
O(5)#1–Mn(3)–N(12)	74.86(8)		
O(7)#1–Mn(3)–N(12)	96.54(10)		
O(7)–Mn(3)–N(12)	95.81(10)		
N(12)#1–Mn(3)–N(12)	163.08(12)		
Mn(1)–O(4)–Mn(2)	127.93(9)		
Mn(3)–O(5)–Mn(1)	129.29(9)		

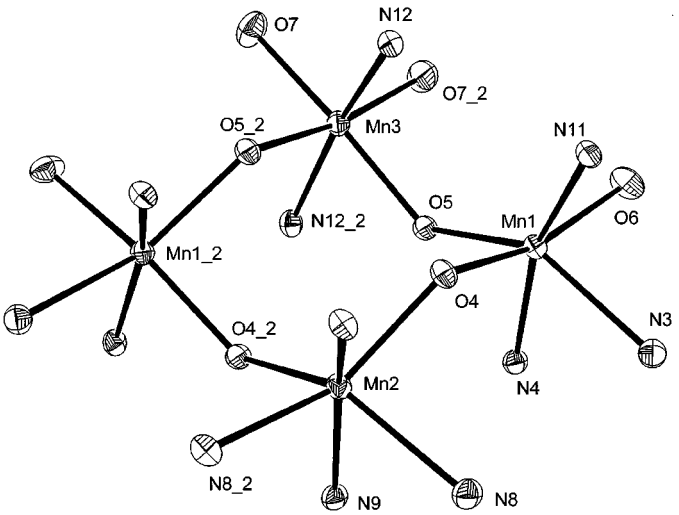

FIG. 2. Mn_4O_4 core structure of **1**.

six-coordinate metal ions (24 binding sites) requires four extra ligands, and water fills this role. The waters are distributed symmetrically with two bound to Mn(3) and one each to the Mn(1) centers, resulting in *cis*-MnN_2O_4 (Mn(3)), *mer*-N_3O_3 (Mn(1)), and *cis*-N_4O_2 (Mn(2)) chromophores.

Crystal Structure of $[Mn_4(po2p)_4(H_2O)_2](ClO_4)_4 \cdot 3H_2O$ (**2**)

A structural representation of the cation in **2**, based on a preliminary structural determination, is shown in Fig. 3. Four pseudo-octahedral Mn(II) centers are bound simultaneously to four deprotonated ligands arranged in a rectangular shape, with two ligands bridging pairs of metals with an N_2 diazine and a terminal alkoxide, and two providing alkoxide bridges. The ligands bridging the edges of the rectangle are tetradentate with one pyridine ring uncoordinated, while those bridging along the sides are pentadentate. Since the bridging alkoxide fills two metal coordination sites two extra ligands (water) are required to complete the six-coordination at each metal center. The core of the structure is shown in Fig. 4.

The manganese centers comprise two different types; MnN_5O (Mn(2)) and *mer*-MnN_3O_3 (Mn(1)) in contrast to the arrangement in **1**. The rectangle is defined by Mn(1)–Mn(2) dimensions of 5.290 and 3.930 Å, with a Mn(1)–O(1)–Mn(2) angle of 127.0°, and a Mn–N–N–Mn torsional angle of 170.3°, indicating a trans arrangement of the two metal centers about the N–N bridge. Mn–N and Mn–O distances fall in the ranges 2.17–2.31 and 2.15–2.23 Å respectively.

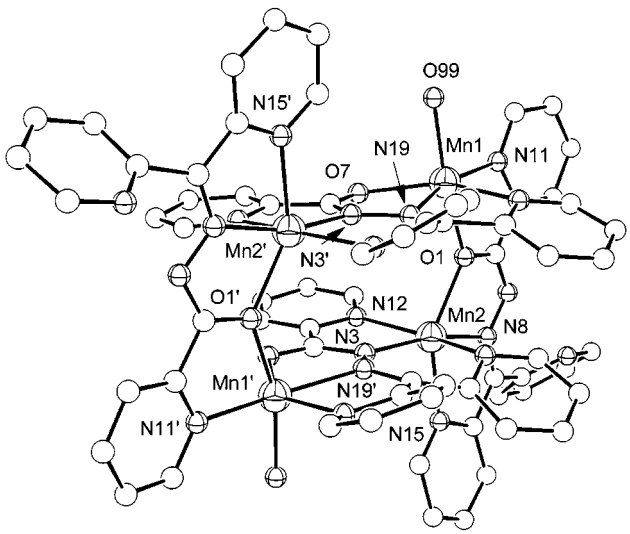

FIG. 3. Structural representation of the cation in **2** (40% probability thermal ellipsoids). Monoclinic, $C2/c$, $a = 22.501(3)$ Å, $b = 15.811(2)$ Å, $c = 26.083(4)$ Å, $\beta = 105.417(2)$, $Z = 4$.

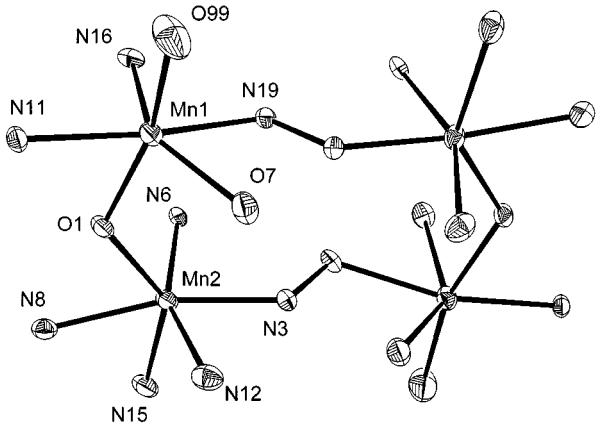

FIG. 4. $Mn_4(N–N)_2O_2$ core structure of **2**.

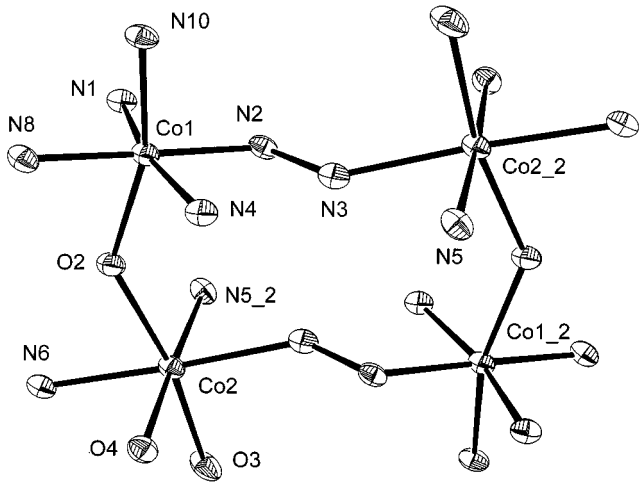

FIG. 6. $Co_4(N–N)_2O_2$ core structure of **3**.

Crystal Structure of $[Co_4(poap\text{-}H)_2(poap\text{-}2H)_2](NO_3)_4 \cdot 7H_2O$ **(3)**

A structural representation of the cation in **3** is shown in Fig. 5, and the core structure is shown in Fig. 6. Selected distances and angles are listed in Table 3. The overall structure bears a close resemblance to that in **2**, with a rectangular arrangement of cobalt centers bridged along the edges by alkoxide and along the sides by diazine N–N groups. Cobalt-ligand distances fall into two well-separated groups with all distances from Co(1) < 1.98 Å, and from Co(2) > 2.08 Å. This is a clear indication that the complex consists of a mixture of two Co(III) (Co(1)) and two Co(II) (Co(2)) centers. This results in the dimensions of the rectangle being significantly smaller in **3** (Co(1)–Co(2), 4.970(2) Å; Co(1)–Co(2)#1, 3.848(2) Å) than in **2**, as would be expected. The ligands comprise two pairs arranged along the edges and the sides of the rectangle. Edge ligands are tetradentate, filling five metal coordination sites through alkoxide bridging (−1 charge), while side ligands are pentadentate, with coordinated and deprotonated amine and diazine nitrogens (N(4), N(2)) (−2 charge). A very short

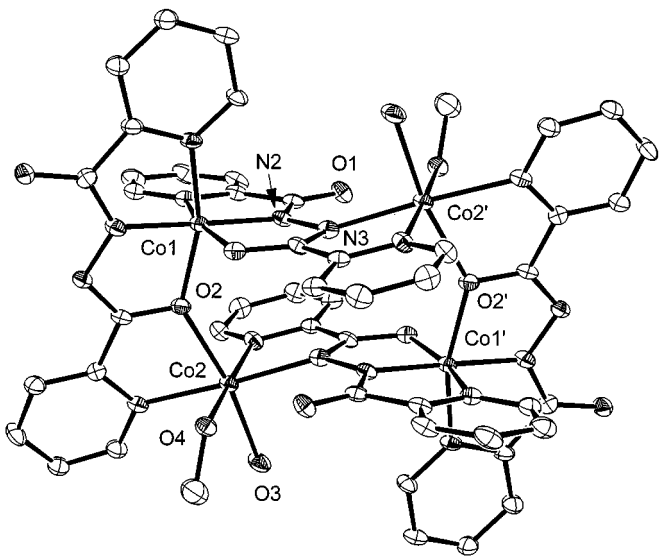

FIG. 5. Structural representation of the cation in **3** (40% probability thermal ellipsoids).

TABLE 3
Bond Lengths (Å) and Angles (°) for $[Co_4(poap\text{-}H)_2(poap\text{-}2H_2](NO_3)_4 \cdot 7H_2O$ (3)

Co(1)–N(8)	1.853(4)	N(8)–Co(1)–N(1)	96.35(19)
Co(1)–N(4)	1.863(4)	N(4)–Co(1)–N(1)	165.49(19)
Co(1)–N(2)	1.874(4)	N(2)–Co(1)–N(1)	83.56(17)
Co(1)–N(10)	1.919(4)	N(10)–Co(1)–N(1)	92.05(17)
Co(1)–N(1)	1.943(4)	N(8)–Co(1)–O(2)	81.00(16)
Co(1)–O(2)	1.975(3)	N(4)–Co(1)–O(2)	92.68(16)
Co(2)–O(4)	2.086(3)	N(2)–Co(1)–O(2)	100.16(15)
Co(2)–O(3)	2.097(4)	N(10)–Co(1)–O(2)	162.87(16)
Co(2)–N(6)	2.134(4)	N(1)–Co(1)–O(2)	87.57(15)
Co(2)–O(2)	2.138(3)	N(5)#1–Co(2)–O(4)	176.52(15)
Co(2)–N(3)#1	2.139(4)	N(5)#1–Co(2)–O(3)	89.26(17)
N(5)–Co(2)#1	2.082(4)	O(4)–Co(2)–O(3)	92.30(15)
Co(1)–Co(2)	3.848(2)	N(5)#1–Co(2)–N(6)	100.64(16)
Co(1)–Co(2)#1	4.879(2)	O(4)–Co(2)–N(6)	82.41(15)
N(8)–Co(1)–N(4)	98.02(19)	O(3)–Co(2)–N(6)	92.32(16)
N(8)–Co(1)–N(2)	178.83(17)	N(5)#1–Co(2)–O(2)	91.52(15)
N(4)–Co(1)–N(2)	82.12(18)	O(4)–Co(2)–O(2)	87.52(14)
N(8)–Co(1)–N(10)	82.03(18)	O(3)–Co(2)–O(2)	169.49(15)
N(4)–Co(1)–N(10)	91.94(18)	N(6)–Co(2)–O(2)	77.23(14)
N(2)–Co(1)–N(10)	96.81(17)	N(5)#1–Co(2)–N(3)#1	78.58(16)
O(4)–Co(2)–N(3)#1	98.28(14)		
O(3)–Co(2)–N(3)#1	90.78(16)		
N(6)–Co(2)–N(3)#1	176.79(14)		
O(2)–Co(2)–N(3)#1	99.65(14)		
Co(1)–O(2)–Co(2)	138.56(18)		

Note. Symmetry transformations used to generate equivalent atoms: #1 $-x+2, -y+2, -z+1$.

C–O distance (C(6)–O(1), 1.267(6) Å) strongly supports this assignment. Four additional coordination sites are filled in the structural sample by two water and two methanol molecules. The mixed Co(II)/Co(III) content and the presence of doubly deprotonated ligands are the result of using cobalt acetate in the sample preparation and exposing the mother liquor to air during crystal growth, leading to partial oxidation of two Co(II) centers.

Crystal Structure of $[Co_4(poapz\text{-}H)_4(H_2O)_4](NO_3)_4 \cdot 2H_2O$ (**4**)

A structural representation of the cation in **4** is shown in Fig. 7, and selected distances and angles are listed in Table 4. This compound is isostructural with **1**, with eclipsed ligands, a square Co_4O_4 grid structure, and waters bound in the same manner. Co–O and Co–N distances fall in the ranges 2.07–2.20 and 2.10–2.26 Å, respectively, consistent with the presence of Co(II) centers. Co–Co distances (Co(1)–Co(2), 3.964(2) Å; Co(1)–Co(3), 3.898(2) Å) and Co–O–Co angles (Co(1)–O(2)–Co(2), 135.9°; Co(1)–O(2)–Co(3), 133.3°) are consistent with square grids with ligands of this sort (20).

Crystal Structure of $[Co_4(pzoapz\text{-}H)_4(H_2O)_4](ClO_4)_4 \cdot 3H_2O$ (**5**)

A structural representation of the cation in **5** is shown in Fig. 8, and the structural core in Fig. 9. Selected distances and angles are listed in Table 5. Four pseudo-octahedral cobalt(II) centers are bound to four ligands arranged in two parallel pairs above and below the Co_4 pseudo-plane, with four alkoxide oxygen atoms bridging the metal ions. The ligands are in an opposed arrangement with NH_2 ends pointing in opposite directions. This leads to a different core structure from **1** and **4**, with two *trans*-CoN_2O_4 centers (Co(2), Co(4)) and two *cis*-CoN_4O_2 centers (Co(1), Co(3)). Each ligand is tetradentate, but fills five metal ion sites due to the alkoxide bridges, and four water molecules act as extra ligands, with two waters bound to Co(2) and Co(4). Co–N and Co–O distances fall in the ranges 1.99–2.19 and 2.01–2.18 Å, typical of six-coordinate Co(II) centers. Co–Co separations are in the range 3.88–3.95 Å, and Co–O–Co angles in the range 133.5°–136.0°.

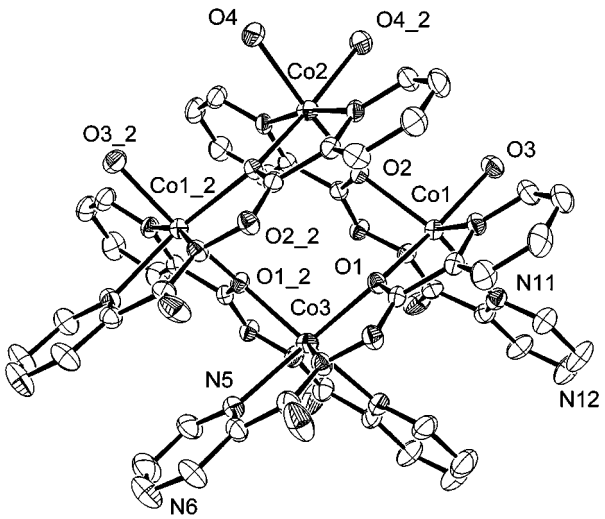

FIG. 7. Structural representation of the cation in **4** (40% probability thermal ellipsoids).

TABLE 4
Bond Lengths (Å) and Angles (°) for $[Co_4(poapz\text{-}H)_4(H_2O)_4](NO_3)_4 \cdot 2H_2O$ (4)

Co(1)–O(1)	2.093(4)	O(1)–Co(3)–O(1)	100.4(2)
Co(1)–O(2)	2.199(4)	O(2)–Co(1)–O(3)	90.5(2)
Co(1)–O(3)	2.099(4)	O(1)–Co(3)–N(3)	74.8(2)
Co(1)– N(1)	2.110(5)	O(2)–Co(1)–N(1)	119.7(2)
Co(1)–N(9)	2.011(5)	O(1)–Co(3)–N(3)	120.6(2)
Co(1)–N(11)	2.258(5)	O(2)–Co(1)–N(9)	74.2(2)
Co(2)–O(2)	2.077(4)	O(1)–Co(3)–N(5)	146.9(2)
Co(2)–O(4)	2.160(4)	O(2)–Co(1)–N(11)	148.9(2)
Co(2)–N(7)	2.084(5)	O(1)–Co(3)–N(5)	88.3(2)
Co(3)–O(1)	2.154(4)	O(3)–Co(1)–N(1)	88.7(2)
Co(3)–N(3)	2.019(5)	O(1)–Co(3)–N(3)	120.6(2)
Co(3)–N(5)	2.258(5)	O(3)–Co(1)–N(9)	96.0(2)
O(1)–Co(1)–O(2)	89.5(2)	O(1)–Co(3)–N(3)	74.8(2)
O(4)–Co(2)–N(7)	91.7(2)	O(3)–Co(1)–N(11)	90.4(2)
O(1)–Co(1)–O(3)	164.9(2)	O(1)–Co(3)–N(5)	88.3(2)
O(1)–Co(1)–N(1)	78.2(2)	N(1)–Co(1)–N(9)	165.5(2)
O(4)–Co(2)–N(7)	95.1(2)	O(1)–Co(3)–N(5)	146.9(2)
O(1)–Co(1)–N(9)	98.6(2)	N(1)–Co(1)–N(11)	91.4(2)
N(7)–Co(2)–N(7)	170.9(3)	N(3)–Co(3)–N(3)	157.8(3)
O(1)–Co(1)–N(11)	97.3(2)	N(9)–Co(1)–N(11)	74.9(2)
N(3)–Co(3)–N(5)	73.3(2)		
O(2)–Co(2)–O(2)	96.0(2)		
N(3)–Co(3)–N(5)	92.5(2)		
O(2)–Co(2)–O(4)	171.4(2)		
O(2)–Co(2)–O(4)	91.0(2)		
N(3)–Co(3)–N(5)	73.3(2)		
O(2)–Co(2)–N(7)	79.4(2)		
N(5)–Co(3)–N(5)	101.7(3)		
O(2)–Co(2)–N(7)	94.4(2)		
Co(1)–O(1)–Co(3)	133.3(2)		
Co(1)–O(2)–Co(2)	135.9(2)		
O(4)–Co(2)–O(4)	82.5(2)		
O(4)–Co(2)–N(7)	95.1(2)		

Crystal Structure of $[Cu_4(poap\text{-}H)_4](ClO_4)_4 \cdot CH_3CN \cdot 4.75H_2O$ (**6**)

A structural representation of the cation in **6** is shown in Fig. 10, and the structural core in Fig. 11. Selected distances and angles are listed in Table 6. Four five-coordinate square-pyramidal Cu(II) centers are arranged in a square Cu_4O_4 alkoxide bridged grid, similar to related systems (20). The CuN_3O_2 square pyramids are defined by four short equatorial bonds, typically < 2.05 Å, with a much longer

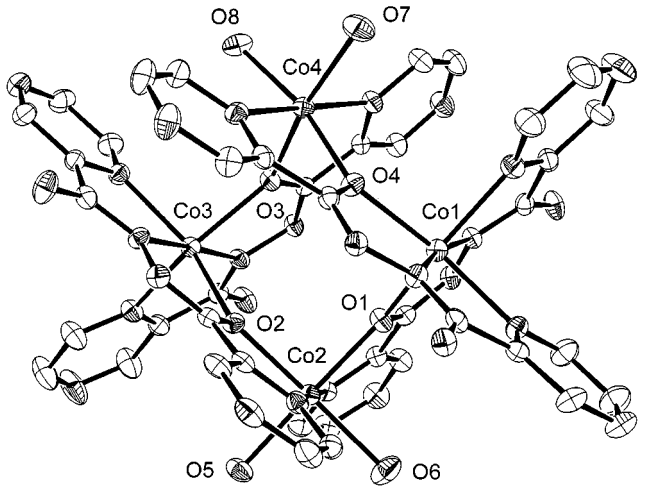

FIG. 8. Structural representation of the cation in **5** (40% probability thermal ellipsoids).

axial bond to the bridging oxygens. This sets up an alternation of the square pyramids, such that each oxygen bridge connects two adjacent copper centers by an orthogonal $d_{x^2-y^2}/d_{z^2}$ contact. This has significant magnetic consequences (*vide infra*). Cu–Cu distances fall in the range 3.92–3.99 Å, and Cu–O–Cu angles in the range 138.3°–139.7°.

Crystal Structure of $[Cu_5(3poap\text{-}H)_3(3poap\text{-}3H)]\ (ClO_4)_4 \cdot 7.5H_2O$ (**7**)

A preliminary structural representation of the cationic fragment in **7** is shown in Fig. 12. The ligand 3poap has a pendant OH group strategically positioned on the pyridine ring adjacent to the main OH group such that if the

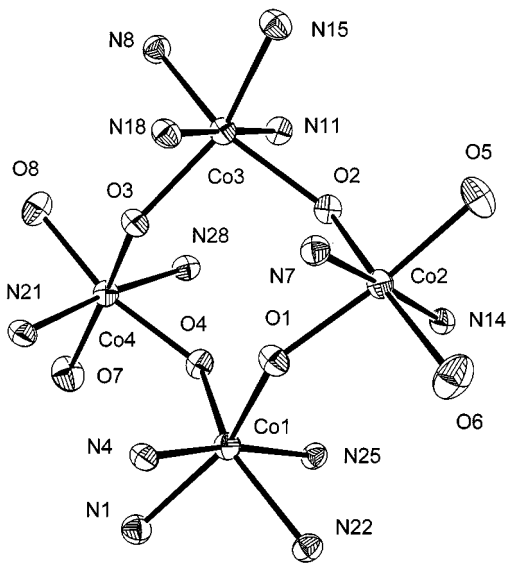

FIG. 9. Co_4O_4 core structure of **5**.

TABLE 5
Bond Lengths (Å) and Angles (°) for $[Co_4(pzoapz\text{-}H)_4(H_2O)_4](ClO_4)_4 \cdot 3H_2O$ (5)

Co(1)–O(1)	2.177(3)	O(7)–Co(4)–N(28)	83.6(1)
Co(1)–O(4)	2.130(3)	O(8)–Co(4)–N(21)	93.2(2)
Co(1)–N(1)	2.187(4)	O(8)–Co(4)–N(28)	91.2(1)
Co(1)–N(4)	1.993(4)	N(21)–Co(4)–N(28)	174.4(1)
Co(1)–N(22)	2.201(4)	Co(1)–O(4)–Co(4)	133.9(1)
Co(1)–N(25)	2.014(4)	Co(1)–O(1)–Co(2)	136.0(1)
Co(2)–O(1)	2.073(3)	Co(2)–O(2)–Co(3)	135.2(1)
Co(2)–O(2)	2.100(3)	Co(3)–O(3)–Co(4)	133.5(1)
Co(2)–O(5)	2.074(4)	O(1)–Co(1)–O(4)	99.0(1)
Co(2)–O(6)	2.130(4)	O(5)–Co(2)–N(14)	90.5(1)
Co(2)–N(7)	2.135(4)	O(1)–Co(1)–N(1)	150.6(1)
Co(2)–N(14)	2.154(4)	O(6)–Co(2)–N(7)	86.8(2)
Co(3)–O(2)	2.168(4)	O(1)–Co(1)–N(4)	75.4(1)
Co(3)–O(3)	2.119(3)	O(6)–Co(2)–N(14)	89.7(2)
Co(3)–N(8)	2.160(4)	O(1)–Co(1)–N(22)	92.8(1)
Co(3)–N(11)	2.007(3)	N(7)–Co(2)–N(14)	176.4(1)
Co(3)–N(15)	2.162(4)	O(1)–Co(1)–N(25)	106.3(1)
Co(3)–N(18)	1.997(3)	O(2)–Co(3)–O(3)	97.0(1)
Co(4)–O(3)	2.105(3)	O(4)–Co(1)–N(1)	91.8(1)
Co(4)–O(4)	2.076(4)	O(2)–Co(3)–N(8)	150.8(1)
Co(4)–O(7)	2.157(4)	O(1)–Co(2)–O(6)	91.6(1)
Co(4)–O(8)	2.037(4)	N(11)–Co(3)–N(18)	177.5(2)
Co(4)–N(21)	2.138(4)	O(1)–Co(2)–N(7)	78.2(1)
Co(4)–N(28)	2.152(4)	N(15)–Co(3)–N(18)	76.2(1)
Co(1)–Co(2)	3.941(2)	O(1)–Co(2)–N(14)	101.0(1)
Co(2)–Co(3)	3.947(2)	O(3)–Co(4)–O(4)	88.2(1)
Co(3)–Co(4)	3.880(2)	O(2)–Co(2)–O(5)	92.2(1)
Co(1)–Co(4)	3.870(2)	O(3)–Co(4)–O(7)	168.9(1)
O(4)–Co(1)–N(4)	116.4(2)	O(2)–Co(2)–O(6)	167.3(1)
O(2)–Co(3)–N(11)	75.1(1)	O(3)–Co(4)–O(8)	87.3(1)
O(4)–Co(1)–N(22)	148.7(1)	O(2)–Co(2)–N(7)	105.9(1)
O(2)–Co(3)–N(15)	95.7(2)	O(3)–Co(4)–N(21)	77.0(1)
O(4)–Co(1)–N(25)	75.0(1)	O(2)–Co(2)–N(14)	77.6(1)
O(2)–Co(3)–N(18)	102.5(1)	O(3)–Co(4)–N(28)	106.8(1)
N(1)–Co(1)–N(4)	75.3(1)	O(5)–Co(2)–O(6)	88.0(2)
O(3)–Co(3)–N(8)	94.1(1)	O(4)–Co(4)–O(7)	90.2(1)
N(1)–Co(1)–N(22)	92.0(2)	O(5)–Co(2)–N(7)	90.3(1)
O(3)–Co(3)–N(11)	105.5(1)	O(4)–Co(4)–O(8)	166.4(1)
N(1)–Co(1)–N(25)	102.9(2)	O(4)–Co(4)–N(21)	98.3(1)
O(3)–Co(3)–N(15)	150.9(1)	O(4)–Co(4)–N(28)	77.8(1)
N(4)–Co(1)–N(22)	94.7(2)	O(7)–Co(4)–O(8)	96.6(2)
O(3)–Co(3)–N(18)	75.6(1)	O(7)–Co(4)–N(21)	92.4(1)
N(4)–Co(1)–N(25)	168.4(2)		
N(8)–Co(3)–N(11)	75.9(2)		
N(22)–Co(1)–N(25)	73.9(1)		
N(8)–Co(3)–N(15)	87.3(2)		
O(1)–Co(2)–O(2)	90.7(1)		
N(8)–Co(3)–N(18)	106.4(2)		
O(1)–Co(2)–O(5)	168.5(1)		
N(11)–Co(3)–N(15)	103.1(1)		

normal square grid forms on one side of the ligand, the other side of each ligand in the cluster will have an "open" N_2O coordination pocket to attract a second shell of metal ions during the self-assembly process. Figure 12 shows the familar Cu_4O_4 core structure (cf. **6**), with two pairs of parallel ligands above and below the metal pseudo-plane defined by

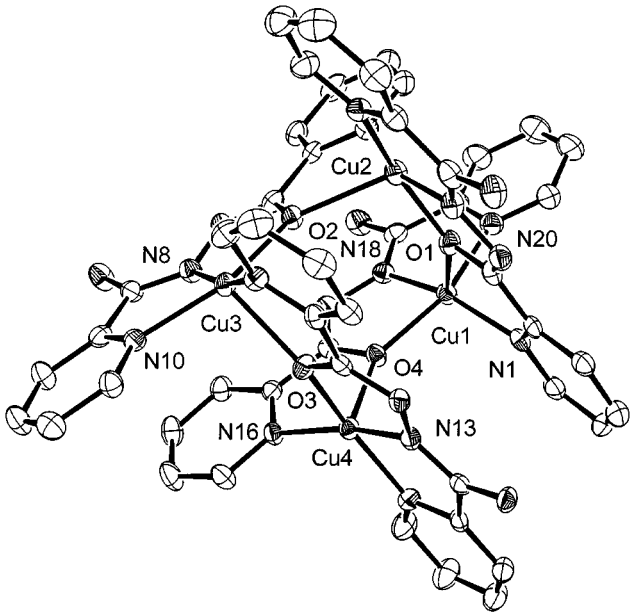

FIG. 10. Structural representation of the cation in **6** (40% probability thermal ellipsoids).

Cu(1), Cu(2), Cu(3), and Cu(4). The metal ions within the core are bridged in the same fashion as in **6**, with an orthogonal connection between each copper via the alkoxide. The Cu_4 core is quite distorted, with a significant tetrahedral twist. Cu–Cu separations fall in the range 3.98–4.17 Å, and Cu–O–Cu angles fall in the range 138.7°–142.4°.

Two ligands are opposed in one pair, while in the other pair they are eclipsed. This leads to a projection of the N_2O

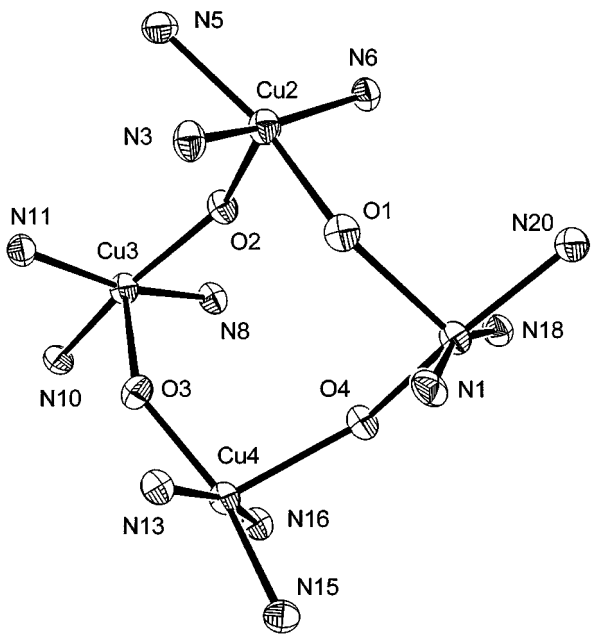

FIG. 11. Mn_4O_4 core structure of **6**.

TABLE 6
Bond Lengths (Å) and Angles (°) for $[Cu_4(poap\text{-}H)_4](ClO_4)_4 \cdot CH_3CN \cdot 4.75H_2O$ (6)

Cu(1)–O(1)	2.209(3)	N(5)–Cu(2)–N(6)	104.77(16)
Cu(1)–O(4)	1.994(4)	O(2)–Cu(3)–O(3)	93.44(14)
Cu(1)–N(1)	1.995(4)	O(2)–Cu(3)–N(8)	79.22(16)
Cu(1)–N(18)	1.904(4)	Cu(1)–O(4)–Cu(4)	139.11(17)
Cu(1)–N(20)	2.040(4)	O(1)–Cu(1)–O(4)	95.86(14)
Cu(2)–O(1)	1.989(3)	N(8)–Cu(3)–N(11)	167.50(16)
Cu(2)–O(2)	2.235(4)	O(1)–Cu(1)–N(1)	78.03(15)
Cu(2)–N(3)	1.905(4)	N(10)–Cu(3)–N(11)	102.71(17)
Cu(2)–N(5)	2.018(4)	O(1)–Cu(1)–N(18)	119.83(16)
Cu(2)–N(6)	2.000(4)	O(3)–Cu(4)–O(4)	98.91(13)
Cu(3)–O(2)	2.007(4)	O(1)–Cu(1)–N(20)	94.72(15)
Cu(3)–O(3)	2.231(3)	O(3)–Cu(4)–N(13)	79.29(16)
Cu(3)–N(8)	1.907(4)	O(4)–Cu(1)–N(1)	96.52(18)
Cu(3)–N(10)	2.050(4)	O(3)–Cu(4)–N(15)	158.69(15)
Cu(3)–N(11)	1.998(4)	O(4)–Cu(1)–N(18)	78.96(17)
Cu(4)–O(3)	1.985(3)	O(3)–Cu(4)–N(16)	96.91(16)
Cu(4)–O(4)	2.214(4)	O(4)–Cu(1)–N(20)	158.62(15)
Cu(4)–N(13)	1.897(4)	O(4)–Cu(4)–N(13)	116.60(16)
Cu(4)–N(15)	2.014(4)	N(1)–Cu(1)–N(18)	161.77(17)
Cu(4)–N(16)	1.978(4)	O(4)–Cu(4)–N(15)	95.42(15)
Cu(1)–Cu(2)	3.924(1)	O(2)–Cu(3)–N(10)	158.11(15)
Cu(2)–Cu(3)	3.982(1)	O(2)–Cu(3)–N(11)	96.45(16)
Cu(3)–Cu(4)	3.942(1)	O(3)–Cu(3)–N(8)	114.24(15)
Cu(4)–Cu(1)	3.944(1)	O(3)–Cu(3)–N(10)	100.90(15)
N(1)–Cu(1)–N(20)	103.8(2)	O(3)–Cu(3)–N(11)	77.53(14)
O(4)–Cu(4)–N(16)	78.18(16)	N(8)–Cu(3)–N(10)	79.83(18)
N(18)–Cu(1)–N(20)	79.66(17)	Cu(1)–O(1)–Cu(2)	138.3(1)
N(13)–Cu(4)–N(15)	80.22(17)	Cu(2)–O(2)–Cu(3)	139.7(2)
O(1)–Cu(2)–O(2)	97.73(13)	Cu(3)–O(3)–Cu(4)	138.4(1)
N(13)–Cu(4)–N(16)	165.05(19)	Cu(4)–O(4)–Cu(1)	139.1(2)
O(1)–Cu(2)–N(3)	78.90(16)		
N(15)–Cu(4)–N(16)	101.42(16)		
O(1)–Cu(2)–N(5)	159.08(15)		
Cu(1)–O(1)–Cu(2)	138.30(18)		
O(1)–Cu(2)–N(6)	95.29(16)		
O(2)–Cu(2)–N(3)	119.97(16)		
O(2)–Cu(2)–N(5)	92.36(15)		
Cu(2)–O(2)–Cu(3)	139.65(17)		
O(2)–Cu(2)–N(6)	77.71(16)		
N(3)–Cu(2)–N(5)	80.19(17)		
N(3)–Cu(2)–N(6)	161.81(19)		
Cu(3)–O(3)–Cu(4)	138.36(17)		

external pockets outside the core. Figure 12 shows just one external copper, Cu(5), bound to a deprotonated NH (N(4)), diazine (N(2)), and 3-hydroxy pyridine (O(1)) sites, with a water molecule (O(26)) as the fourth ligand. The short carbonyl bond (C(6)–O(2), 1.267 Å) confirms this assignment, and indicates that the ligand in question loses three protons. Cu(5) is connected to Cu(2) by a *trans* diazine bridge (Cu(2)–N(3)–N(2)–Cu(5), torsional angle 176.0°). The extra copper-based electron density amounted to ~0.3 copper atoms in total. This would not lead to a significant difference regarding the molecular formula (see Experimental), or the magnetic properties (*vide infra*). Figure 13 shows a full complement of copper centers, with Cu(6),

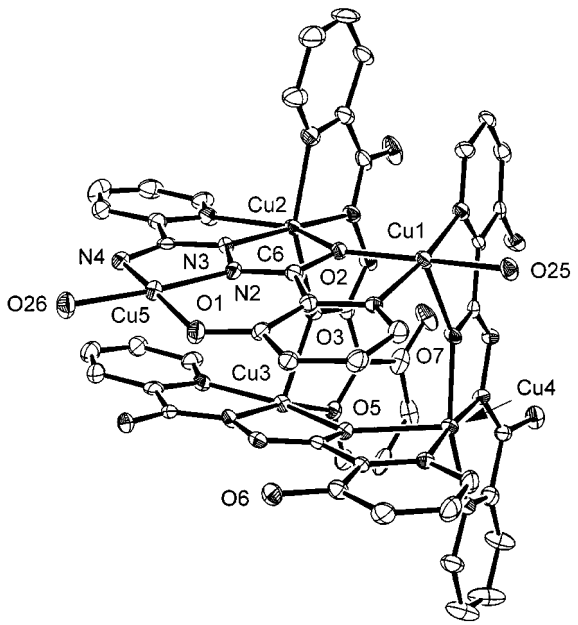

FIG. 12. Structural representation of the cation in **7** (40% probability thermal ellipsoids), just illustrating the fully occupied copper centers.

Cu(7), and Cu(8) all occupying comparable sites to Cu(5). It is of significance that additional oxygen ligand sites were also revealed at sensible bonding distances to these partially occupied copper centers.

Self-Assembly

Ligands with a substituted 2-picolylhydrazide or 2-pyrazine carboxylic acid hydrazide backbone (Scheme 1), and contiguous coordination pockets capable of producing five-membered chelate rings on bonding to transition-metal centers, e.g., poap, poapz, pzoapz, in general undergo high-yield self-assembly reactions to produce square and rectangular tetranuclear grids (20). The current group of ligands

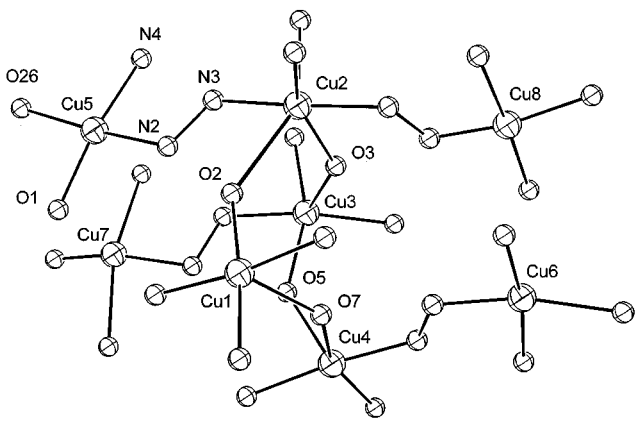

FIG. 13. Core structure of **7** showing locations of all eight copper centers.

produce square $M_4(\mu\text{-O})_4$ alkoxide-bridged grids with Mn(II), Co(II), and Cu(II) salts, and rectangular mixed bridge grids, $M_4(\mu\text{-O})_2(\mu\text{-N-N})_2$, with Mn(II) salts, and in a special situation with a Co(II)/Co(III) combination resulting from aerial oxidation. A mechanism for self-assembly is hard to pinpoint, but precoordination of a metal ion on one side of the ligand in a NO or N_2O pocket, with extra coordination sites occupied by solvent molecules, would produce a viable building block. The sequential docking of such subunits would then proceed to construct the grid in a square or rectangular arrangement based on the matching of the positions of the pockets, and the octahedrally based bond angles around the metals themselves. The ultimate subtle differences in resulting grid conformations may rest with subtle differences in the ligands themselves. Po2p and 3poap are similar to the other ligands in that they have the required elements for grid formation. In both cases primary grids are produced, with po2p resulting in a mixed bridged rectangular tetra-manganese cluster. 3-Poap is clearly a special case, and the extra design feature of an external ligand compartment, based on the 3-hydroxy pyridine fragment, points to a capability of selective ligand design with a desired cluster outcome. The elements of the "expected" octanuclear cluster are clearly in evidence, but the difficulties involved in pre-organization of the building blocks prior to self-assembly indicate that the three-dimensional interlocking of the components is as complicated as the assembly of an intricate 3-dimensional puzzle with many complex subunits. Efforts are underway to increase the metal load with 3-poap with copper and other transition-metal ions.

Magnetic Properties

Compound **1** shows an increase in susceptibility (χ_M) as temperature is decreased with a sharp shoulder at $\sim$15 K, indicative of intramolecular antiferromagnetic coupling. A plot of μ (per mole) (Fig. 14) shows that μ_{mol} drops steadily from 11.4 μ_B at 300 K to 3.5 μ_B at 4.5 K. The variable temperature magnetic data were fitted to an exchange expression (see Eqs. [2] and [3] below) derived from the appropriate isotropic exchange Hamiltonian (see Eq. [1] below) for a square arrangement of four $S = \frac{5}{2}$ metal centers (χ_M is the molar susceptibility, ρ is the fraction of paramagnetic impurity, TIP is temperature-independent paramagnetism, θ is a Weiss-like temperature correction; all other terms have their usual significance):

$$H = -2J(S_1S_2 + S_2S_3 + S_3S_4 + S_1S_4) \qquad [1]$$

$$\chi_{M'} = \frac{N\beta^2g^2}{3k(T-\theta)} \frac{\sum S_T(S_T+1)(2S_T+1)\,e^{-E(S_T)/kT}}{\sum S_T(2S_T+1)\,e^{-E(S_T)/kT}} \qquad [2]$$

$$\chi_M = \chi_{M'}(1-\rho) + \frac{2N\beta^2g^2\rho}{3kT} + \text{TIP}. \qquad [3]$$

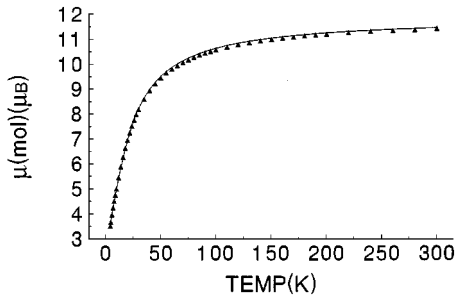

FIG. 14. Variable temperature magnetic data for **1**. The solid line represents the best fit to Eq. [3] ($S = \frac{5}{2}$), with $g = 1.99$, $J = -2.85(4)\,cm^{-1}$, $\rho = 0.014$, $\theta = 0$ K, TIP = 0 emu.mol^{-1} ($10^2R = 1.0$; $R = [\Sigma(\chi_{obs.} - \chi_{calc.})^2/\Sigma\chi^2_{obs}]^{1/2}$).

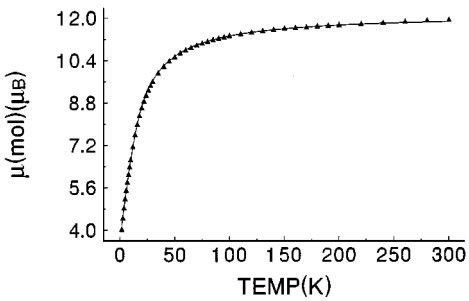

FIG. 15. Variable temperature magnetic data for **2**. The solid line represents the best fit to the exchange expression derived from Eq. [4] ($S = \frac{5}{2}$), with $g = 2.00$, $J_1 = -1.9(2)\,cm^{-1}$, $J_2 = -0.1(1)\,cm^{-1}$, $\rho = 0.037$, TIP = 0 emu.mol^{-1} ($10^2R = 0.60$; $R = [\Sigma(\chi_{obs.} - \chi_{calc.})^2/\Sigma\chi^2_{obs}]^{1/2}$).

For simplicity the model assumes that all exchange integrals between adjacent pairs of Mn(II) centers are the same. The solid line in Fig. 14 represents the best fit of the data to Eq. [3] and was calculated for $g = 1.99(1)$, $J = -2.85(4)\,cm^{-1}$, $\rho = 0.014$, $\theta = 0$ K, TIP = 0 emu (per mole), $10^2R = 1.0$ ($R = [\Sigma(\chi_{obs.} - \chi_{calc.})^2/\Sigma\chi^2_{obs}]^{1/2}$). The negative J value confirms the intramolecular antiferromagnetic coupling. The structure shows that all the manganese(II) centers are linked by alkoxide bridges, with Mn–O–Mn bridge angles in the range 128°–129.5°, typical for antiferromagnetic exchange.

Compound **2** shows a similar profile of μ_{mol} from 2–300 K (Fig. 15) indicative of intramolecular antiferromagnetic exchange. The susceptibiblity data were fitted to an appropriate exchange expression derived as described above from a spin Hamiltonian

$$H = -2J_1(S_1S_2 + S_3S_4) - 2J_2(S_2S_3 + S_1S_4) \qquad [4]$$

appropriate to a rectangle of four $S = \frac{5}{2}$ centers.

A very good data fit was obtained with $g = 2.00$, $J_1 = -1.9(2)\,cm^{-1}$, $J_2 = -0.1(1)\,cm^{-1}$, $\rho = 0.037$, TIP = 0 emu.mol^{-1}, $10^2R = 0.60$ ($R = [\Sigma(\chi_{obs.} - \chi_{calc.})^2/\Sigma\chi^2_{obs}]^{1/2}$). The solid line in Fig. 15 was calculated with these values. Two negative J values are consistent with the structure, which shows a Mn–O–Mn angle of 127.0°, and a Mn–N–N–Mn torsional angle of 170.3°. J_1 is tentatively assigned to the Mn–O–Mn bridging interaction, in reasonable agreement with the properties of **1**, which has a comparable Mn–O–Mn angle. The *trans* arrangement of Mn(II) centers about the N–N bridge would be expected to produce antiferromagnetic coupling (32).

Compound **3** has a magnetic moment that varies over a very narrow range from 2 to 300 K (6.6 μ_B at 2 K, 7.6 μ_B at 300 K), consistent with the presence of two Co(II) (high spin) and two Co(III) (low spin) centers, with essentially no coupling between the Co(II) spins. This result confirms the diagonal placement of each like cobalt center as indicated from the X-ray structure. A very different magnetic result was obtained for **4**, with a molar magnetic moment of 10.0 μ_B at 300 K, which drops slightly to 9.5 μ_B at 100 K and then precipitously to a value of 4.1 μ_B at 2 K. This clearly indicates the presence of significant intramolecular antiferromagnetic exchange, consistent with the [$Co_4(\mu$-O)$_4$] alkoxide-bridged structure. Magnetic data for **5** (Fig. 16) are very similar with a molar moment of 9.4 μ_B at 300 K dropping to 3.5 μ_B at 5 K. The data for **5** were fitted to an isotropic exchange expression (Eq. [3], $S = \frac{3}{2}$) for a square arrangement of four $S = \frac{3}{2}$ centers, and surprisingly a very good fit was obtained for $g = 2.42(1)$, $J = -6.95(4)\,cm^{-1}$, $\rho = 0.004$, TIP = 0.00120 emu.mol^{-1} ($10^2R = 1.20$ ($R = [\Sigma(\chi_{obs.} - \chi_{calc.})^2/\Sigma\chi^2_{obs}]^{1/2}$). The solid line in Fig. 16 is calculated with these parameters. The negative J value indicates intramolecular antiferromagnetic coupling, consistent with the alkoxide-bridged square structure, and large Co–O–Co bridge angles. The data fit for **4** was less satisfactory, but an estimate of $J = -7.0\,cm^{-1}$ is consistent with the same structural motif.

The magnetic data for **6** have been reported already (20) and show that intramolecular exchange is dominated by

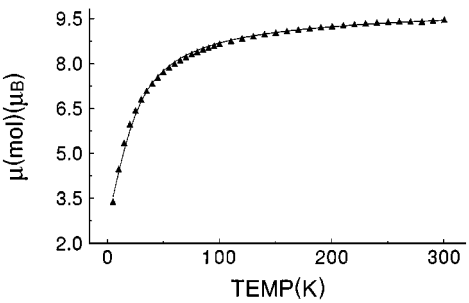

FIG. 16. Variable temperature magnetic data for **5**. The solid line represents the best fit to the exchange expression derived from Eq. [3] ($S = \frac{3}{2}$), with $g = 2.42(1)$, $J = -6.95(4)\,cm^{-1}$, $\theta = 0$, $\rho = 0.004$, TIP = 0.00120 emu.mol^{-1} ($10^2R = 1.20$; $R = [\Sigma(\chi_{obs.} - \chi_{calc.})^2/\Sigma\chi^2_{obs}]^{1/2}$).

ferromagnetic interactions within the Cu_4O_4 square ($J = 7.28(9)\,cm^{-1}$). Magnetic data for the current sample show an almost identical profile of μ_{mol} versus temperature, and a good fit of the data to Eq. [3] ($S = \frac{1}{2}$) gives $g = 2.136(5)$, $J = 6.80(2)\,cm^{-1}$, $\theta = -2$ K, $\rho = 0.016$, TIP = 0.000240 emu.mol^{-1}, $10^2R = 1.5$. The strict orthogonality of the copper magnetic orbitals in **6**, associated with the unusual long/short Cu–O contacts within the square grid, combined with short Cu–Cu contacts ($\sim$4 Å), must lead to a situation where direct antiferromagnetic coupling is nonexistent, but ferromagnetic coupling is possible. This phenomenon has now been demonstrated in square Cu_4O_4 grids (20), in Cu_9O_{12} 3×3 square portcullis-like grids (33), and in a Cu_8O_8 "pinwheel" cluster (34), involving related ligands providing alkoxide bridges between the copper(II) centers.

Compound **7** displays rather unusual magnetic properties. The magnetic moment per mole shows a decrease from 3.9 μ_B at 300 K to 3.15 μ_B at $\sim$35 K, followed by an increase at lower temperatures (Fig. 17). The drop in moment from 300 K would signify the presence of an intramolecular antiferromagnetic component, while the sharp rise at low temperature is indicative of ferromagnetic exchange. A close examination of the structure reveals that within the pseudo-square Cu_4O_4 core all bridging connections are strictly orthogonal, while the connection between Cu(2) and Cu(5) is nonorthogonal through the diazine N–N linkage (N(2)–N(3)). The almost *trans* disposition of Cu(2) and Cu(5) via this bridge would dictate that coupling between Cu(2) and Cu(5) should be antiferromagnetic, and moderately strong (32). Given the connections between Cu(2) and the surrounding copper centers Cu(1), Cu(3), and Cu(5), the Cu(2)–Cu(5) exchange route would be considered to dominate. On this basis the five coppers can realistically be separated into two groups as far as the overall exchange picture is concerned, i.e., Cu(2)–Cu(5) and Cu(1)–Cu(4)–Cu(3). The magnetic data were therefore fitted to a simple exchange expression that is the sum of two terms: a dinuclear term (J_2, Cu(2)–Cu(5)), and an effective linear trinuclear term (J_1, Cu(1)–Cu(4)–Cu(3)). The Hamiltonian

$$H = -2J_1(S_1S_4 + S_3S_4) - 2J_2(S_2S_5) \qquad [5]$$

assumes that coupling between Cu(1) and Cu(3) can be ignored. A good data fit was obtained to the theoretical exchange expression derived from Eq. [5] for $g = 2.06(1)$, $J_1 = 1.9(1)\,cm^{-1}$, $J_2 = -90(2)\,cm^{-1}$, $\rho = 0.035$, TIP = $0.000300\,cm^2\,mol^{-1}$, $10^2R = 0.60$. The solid line in Fig. 17 represents this data fit. J_1 defines a ferromagnetic interaction, within the triangular grouping of coppers, consistent with the properties of all the Cu_4 square systems in this class examined already (20), in which strict orthogonality exists between the metals. The large negative J_2 clearly defines the *trans* N–N linkage between Cu(2) and Cu(5) as a dominant intramolecular antiferromagnetic interaction, entirely consistent with previous results on dicopper(II) systems, where a linear correlation was observed between J and the rotational angle of the copper magnetic planes about the N–N bond. At large angles approaching 180°, $2J$ values around $-200\,cm^{-1}$ were observed (32).

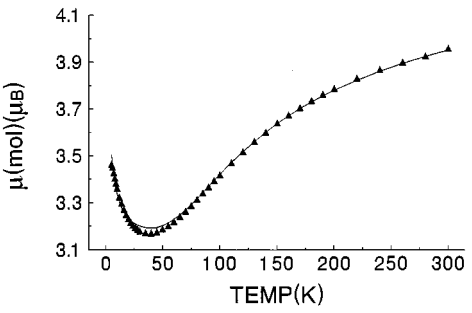

FIG. 17. Variable temperature magnetic data for **7**. The solid line represents the best fit to the exchange expression derived from Eq. [5] for $g = 2.06(1)$, $J_1 = 1.9(1)\,cm^{-1}$, $J_2 = -90(2)\,cm^{-1}$, $\rho = 0.035$, TIP = $0.000300\,cm^2.mol^{-1}$ ($10^2R = 0.60$; $R = [\Sigma(\chi_{obs.} - \chi_{calc.})^2/\Sigma\chi^2_{obs}]^{1/2}$).

ACKNOWLEDGMENTS

We thank the Natural Sciences and Engineering Research Council (Canada), and EPSRC (UK) for financial support, and Dr. R. McDonald (University of Alberta) for structural data for compounds **6** and **7**.

REFERENCES

1. A. Caneschi, A. Cornia, A. C. Fabretti, and D. Gatteschi, *Angew. Chem. Int. Ed.* **38,** 1295 (1999).
2. G. L. Abbati, A. Cornia, A. C. Fabretti, A. Caneschi, and D. Gatteschi, *Inorg. Chem.* **37,** 1430 (1998).
3. M. A. Bolcar, S. M. J. Aubin, K. Folting, D. N. Hendrickson, and G. Christou, *J. Chem. Soc. Chem. Commun.* 1485 (1997).
4. A. Tsohos, S. Dionyssopoulou, C. P. Raptopoulou, A. Terzis, E. G. Bakalbassis, and S. P. Perlepes, *Angew. Chem. Int. Ed.* **38,** 983 (1999).
5. A. J. Blake, C. M. Grant, S. Parsons, J. M. Rawson, and R. E. P. Winpenny, *J. Chem. Soc. Chem. Commun.* 2363 (1994).
6. K. L. Taft, C. D. Delfs, G. C. Papaefthymiou, S. Foner, D. Gatteschi, and S. J. Lippard, *J. Am. Chem. Soc.* **116,** 823 (1994).
7. F. E. Mabbs, E. J. L. McInnes, M. Murrie, S. Parsons, G. M. Smith, C. C. Wilson, and R. E. P. Winpenny, *J. Chem. Soc. Chem. Commun.* 643 (1999).
8. S. M. J. Aubin, Z. Sun, I. A. Guzei, A. L. Rheingold, G. Christou, and D. N. Hendrickson, *J. Chem. Soc. Chem. Commun.* 2239 (1997).
9. Z. Sun, D. Ruiz, N. R. Dilley, M. Soler, J. Ribas, K. Folting, M. B. Maple, G. Christou, and D. N. Hendrickson, *J. Chem. Soc. Chem. Commun.* 1973 (1999).
10. S. M. J. Aubin, S. Spagna, H. J. Eppley, R. E. Sager, G. Christou, and D. N. Hendrickson, *J. Chem. Soc. Chem. Commun.* 803 (1998).
11. M.-T. Youinou, N. Rahmouni, J. Fischer, and J. A. Osborn, *Angew. Chem. Int. Ed. Engl.* **31,** 733 (1992).
12. G. S. Hanan, D. Volkmer, S. S. Ulrich, J.-M. Lehn, G. Baum, and D. Fenske, *Angew. Chem. Int. Ed. Engl.* **36,** 1842 (1997).
13. D. M. Bassani, J.-M. Lehn, K. Fromm, and D. Fenske, *Angew. Chem. Int. Ed. Engl.* **37,** 2364 (1998).

14. O. Waldmann, J. Hassmann, P. Müller, G. S. Hanan, D. Volkmer, U. S. Schubert, and J.-M. Lehn, *Phys. Rev. Lett*. **78,** 3390 (1997).
15. O. Waldmann, J. Hassmann, P. Müller, G. S. Hanan, D. Volkmer, U. S. Schubert, and J.-M. Lehn, *Phys. Rev. B* **58,** 3277 (1998).
16. J. Rojo, J.-M. Lehn, G. Baum, D. Fenske, O. Waldmann, and P. Müller, *Eur. J. Inorg. Chem.* 517 (1999).
17. C.-Y. Duan, Z.-H. Liu, X.-Z. You, F. Xue, and T. W. C. Mak, *J. Chem. Soc. Chem. Commun.* 381 (1997).
18. H. Cheng, D. Chun-ying, F. Chen-jie, L. Yong-jiang, and M. Qing-jin, *J. Chem. Soc. Dalton Trans.* 1207 (2000).
19. C. S. Campos-Fernández, R. Clérac, and K. R. Dunbar, *Angew. Chem. Int. Ed. Engl.* **38,** 3477 (1999).
20. C. J. Matthews, K. Avery, Z. Xu, L. K. Thompson, L. Zhao, D. O. Miller, K. Biradha, K. Poirier, M. J. Zaworotko, C. Wilson, A. E. Goeta, and J. A. K. Howard, *Inorg. Chem.* **38,** 5266 (1999).
21. D. S. Brown, V. H. Crawford, J. W. Hall, and W. E. Hatfield, *J. Phys. Chem.* **81,** 1303 (1977).
22. J. Cosier and A. M. Glazer, *J. Appl. Cryst*. **19,** 105 (1986).
23. (a) Siemens, "SMART Data Collection Software," Ver. 4.050. Siemens Analytical X-ray Instruments Inc., Madison, WI, 1996. (b) Siemens, "SAINT Data Reduction Software," Version 4.050; Siemens Analytical X-ray Instruments Inc., Madison, WI, 1996.
24. G. M. Sheldrick, "SHELXTL 5.04/VMS, An Integrated System for Solving, Refining and Displaying Crystal Structures from Diffraction Data." Siemens Analytical X-ray Instruments Inc., Madison, WI, 1995.
25. G. M. Sheldrick, "SADABS. Empirical Absorption Correction Program." University of Göttingen: Göttingen, Germany, 1996.
26. *SIR92*: A. Altomare, M. Cascarano, C. Giacovazzo, and A. Guagliardi, *J. Appl. Cryst*. **26,** 343 (1993).
27. *DIRDIF94*: P. T. Beurskens, G. Admiraal, G. Beurskens, W. P. Bosman, R. de Gelder, R. Israel, and J. M. M. Smits, The DIRDIF-94 program system, Technical Report of the Crystallography Laboratory, University of Nijmegen, The Netherlands, 1994.
28. D. T. Cromer and J. T. Waber, "International Tables for X-ray Crystallography," Vol. IV, Table 2.2 A. Kynoch Press, Birmingham, England, 1974.
29. J. A. Ibers and W. C. Hamilton, *Acta Crystallogr*. **17,** 781 (1964).
30. *teXsan for Windows*: Crystal Structure Analysis Package, Molecular Structure Corporation, 1997.
31. G. M. Sheldrick, "SHELX97," 1997.
32. L. K. Thompson, Z. Xu, A. E. Goeta, J. A. K. Howard, H. J. Clase, and D. O. Miller, *Inorg. Chem.* **37,** 3217 (1998).
33. L. Zhao, Z. Xu, L. K. Thompson, S. L. Heath, D. O. Miller, and M. Ohba, *Angew. Chem. Int. Ed. Engl.* **39,** 3114 (2000).
34. L. K. Thompson and Z. Xu, unpublished results.